Anion-modulated bifunctional electrocatalytic activity of nickel telluride/cobalt telluride mesoporous nanosheets for high-efficiency and stable overall water splitting

Yagya Raj Rosyara[a], Ishwor Pathak[ac], Alagan Muthurasu[a], Debendra Acharya[a] ,Kisan Chhetri[a], Taewoo Kim[a], Milan Babu Poudel[d], Gunendra Prasad Ojha[e], Tae Hoon Ko*[a] [b] Hak Yong Kim*[a] [b]

[a] *Department of Nano Convergence Engineering, Jeonbuk National University, Jeonju 561-756, Republic of Korea*

[b] *Department of Organic Materials and Fiber Engineering, Jeonbuk National University, Jeonju 561-756, Republic of Korea*

[c]*Department of Chemistry, Amrit Campus, Tribhuvan University, Kathmandu 44613, Nepal*

[d]*Department of Convergence Technology Engineering, Jeonbuk National University 567 Baekje-daero, Deokjin-gu, Jeonju-si, Jeollabuk-do 54896, Republic of Korea*

[e]*Department of Chemistry and Physics, Prairie View A&M University, Prairie View, TX 77446, USA*

Corresponding Author's Email: khy@jbnu.ac.kr, kth1745@jbnu.ac.kr

Materials:

Cobalt Nitrate hexahydrate (Co $(NO_3)_2.6H_2O$), Sigma-Aldrich), Nickel Nitrate hexahydrate (Ni $(NO_3)_2.6h_2O$), Sigma Aldrich), 2-Methylimidazole ($C_4H_6N_2$), Sodium tellurite (Na_2TeO_3, Sigma-Aldrich) were used without further purification. Methanol (99.8%), Ethanol (99.5%), and nitric acid (HNO_3, 60.0 %) were obtained from Samchum Co.Ltd., Seoul Korea. Deionized (DI) water purified through a Millipore-Q system was used to form aqueous solutions during the experiment.

Electrochemically active surface area (ECSA):

The ECSA was calculated from the electrochemical double layer capacitance (Cdl) of the electrode via CV scan conducted in a non-Faradic region at different scan rates from 10 to 100 mV s^{-1} for OER. The Cdl was obtained from the slope of the curve of scan rate (mV s-1) versus current density (mA). The specific capacitance (Cdl) was calculated as :

$$C_{dl} = \frac{|Ja - jc|}{2v}$$

Where v is the scan rate for testing CV, j_a and j_c are the anodic and cathodic current densities.

$$ECSA = \frac{Specific\ capacitance\ (Cdl)}{Cs}$$

Where, C_s is the specific capacitance (0.04 mF cm^{-2}) in 1 M KOH electrolyte.

The roughness factor (RF) values were calculated as:

$$RF = \frac{ECSA}{Sgeo}$$

S_{geo} is the geometric area of the electrode that is 1 cm^2

Electrochemical Impedance spectroscopy (EIS) measurements:

Electrochemical impedance spectroscopy (EIS) was carried out in 1.0 M KOH electrolyte to investigate the reaction kinetics. The measurements were conducted at frequency ranging from 0.01 Hz to 100 kHz. The resulting impedance spectra were analyzed by fitting to an equivalent circuit model. The model includes a series resistance (Rs), which accounts for the ionic resistance of the electrolyte between working and reference electrodes. In parallel, the model features a charge transfer resistance (Rct), reflecting the barrier to electron transfer at the electrode-electrolyte interface, and a capacitance (C), which mimics the double-layer capacitance arising from charge separation at the interface. Together, these elements provide valuable information on the interfacial charge transfer processes and surface

properties of the catalyst during HER and OER.

Calculation of Faradic efficiency (ηF):

The Fradic efficiency of the alkaline elctrolyzer using P-doped $NiTe_2/CoTe_2$ as both anode and cathode was assessed by measuring the volume of evolved O_2 H_2 gas in a lab made H-Cell. The H-cell electrolyzer operated at a current density of 10 mA cm^{-2} for up to 120 minutes. The theoretical volumes of evolved H_2 and O_2 gases were estimated using faraday's law:

$$V_{Theoretical} = \frac{IRTt}{PzF}$$

$T_{Theoretical}$ = Theoretical volume of gas evolution

I = operating current density (mA cm^{-2})

R = universal gas constant (0.0821 atm. L mol^{-1} k^{-1})

t = operating time in second (s)

T= temperature on the kelvin scale (K)

p= pressure (atm)

z = number of electrons involved in the production of 1 mole of O_2(z=4) or H_2(z=2)

F= Faraday's constant (F= 96485 C)

nF can be determined from the following equation: the ratio of the exact volume of real gas ($V_{experimental}$) to the theoretical volume ($V_{theoretical}$) during the reaction.

$$nF = \frac{Vexperimental}{Vtheoretical}$$

where $V_{Experimental}$ is the volume of O_2 and H_2 gas evolved under a pressure of 1 atm at 300 K upon applying a current density of 10 mA Cm^{-2}.

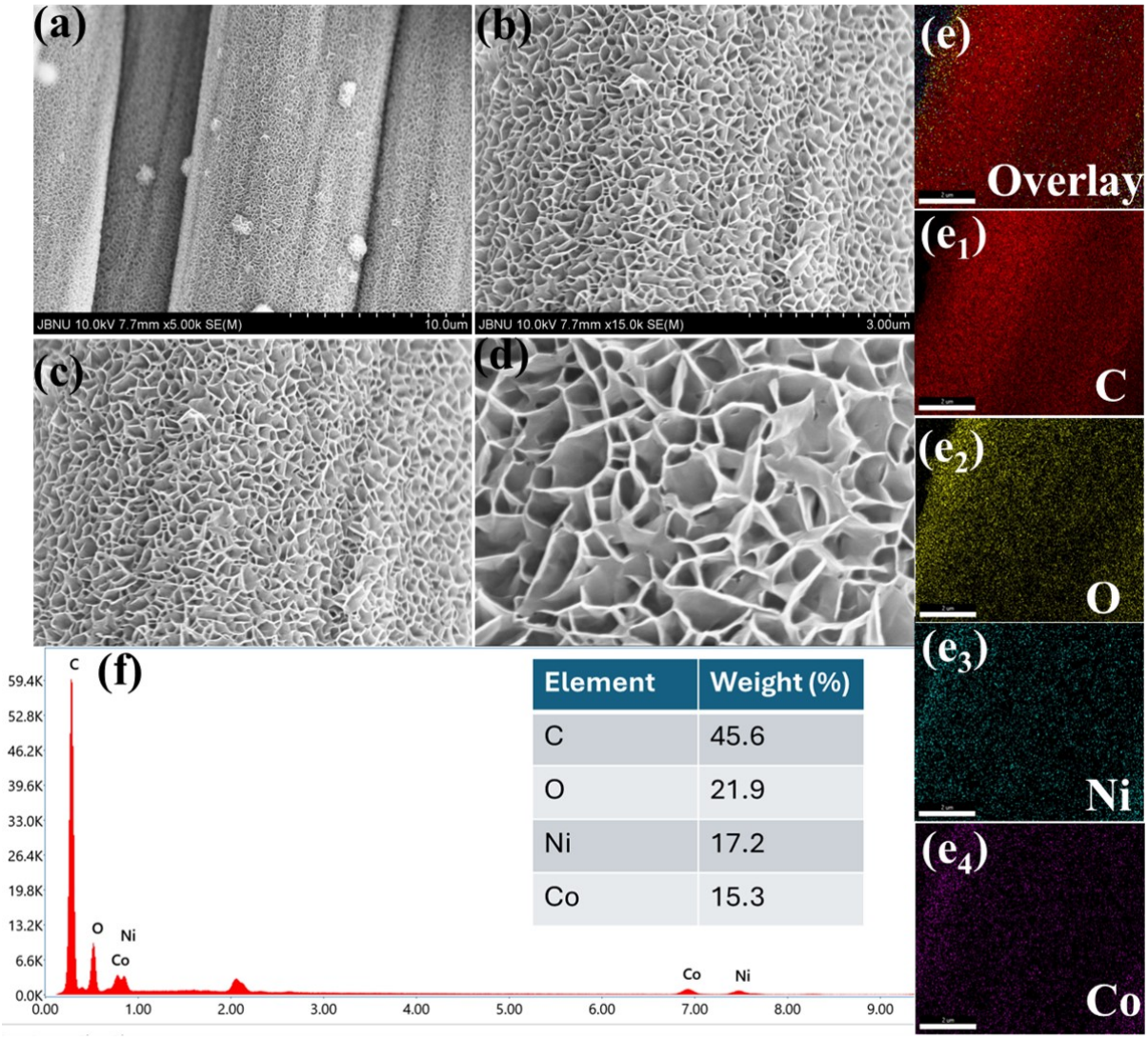

Figure S1. Low and high resolution FESEM image, EDX spectrum and corresponding elemental mapping of NiCo-LDH

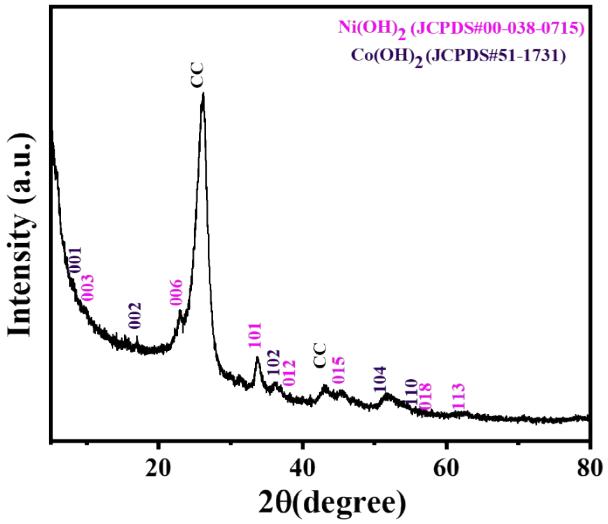

Figure S2. XRD pattern of NiCo-LDH@CC

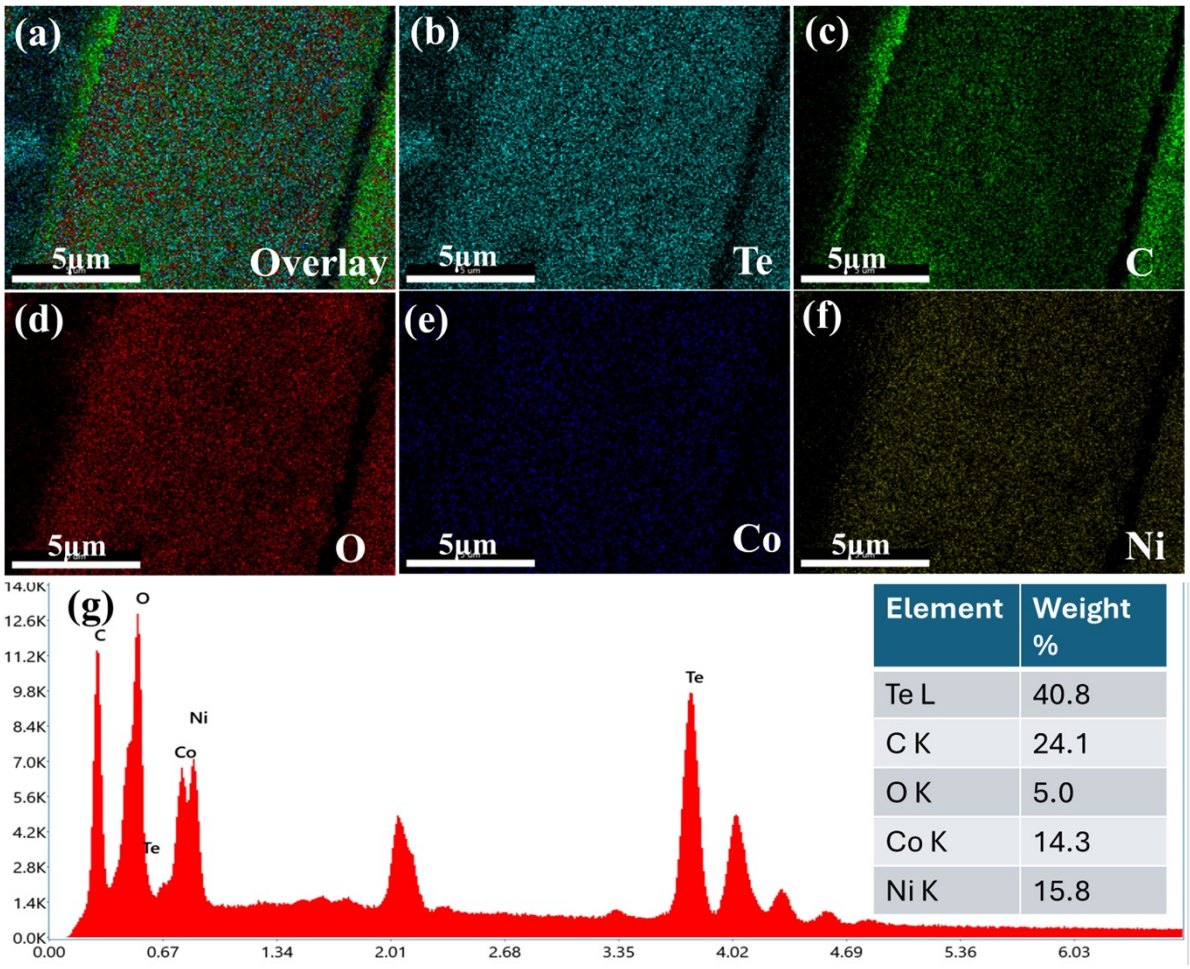

Element	Weight %
Te L	40.8
C K	24.1
O K	5.0
Co K	14.3
Ni K	15.8

Figure S3. FESEM EDX spectra and corresponding elemental mapping of $NiTe_2/COTe_2$@CC

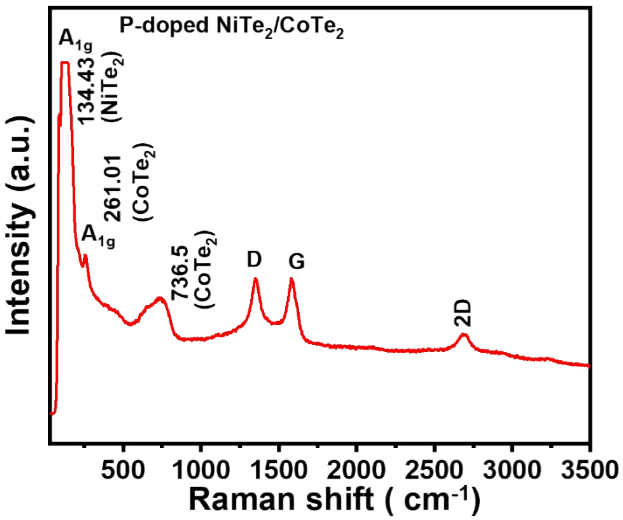

Figure S4. Raman Spectra of P-doped $NiTe_2/CoTe_2$@CC before stability

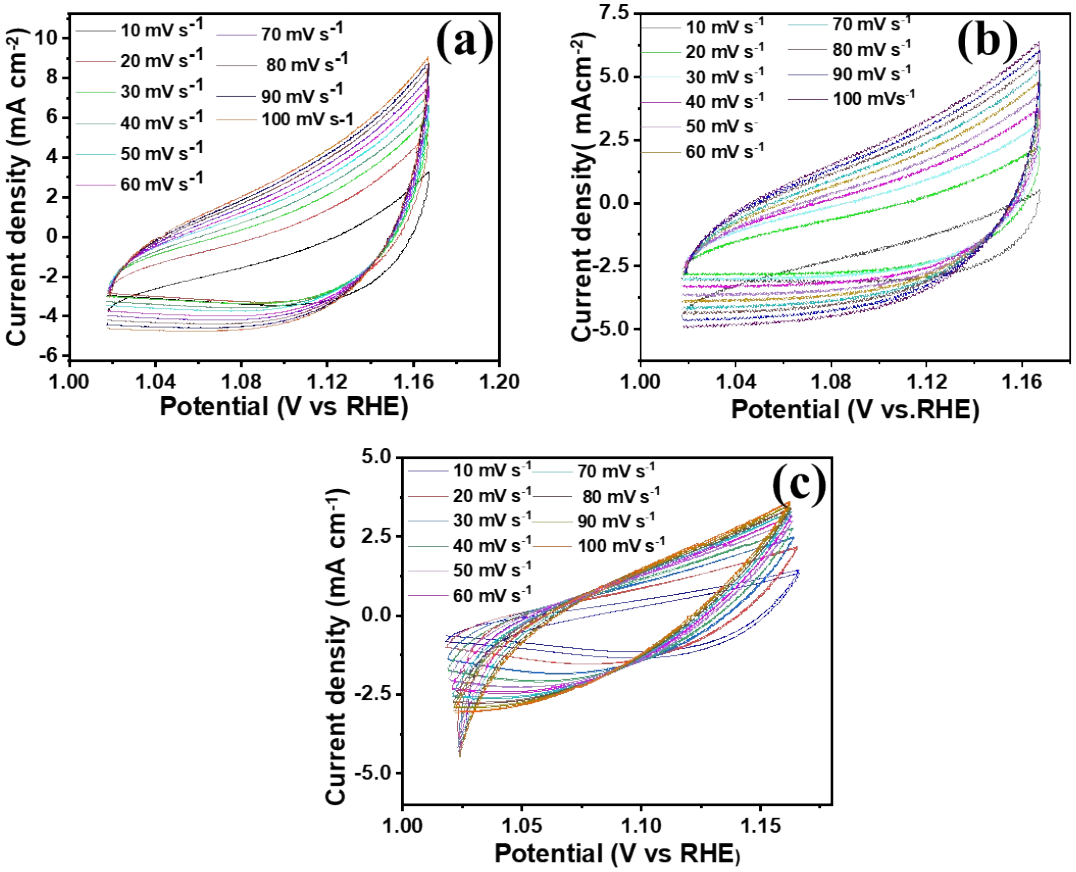

Figure S5. charging capacitance current of (a) P-doped $NiTe_2/CoTe_2$@CC, (b) $NiTe_2/CoTe_2$@CC, (c) NiCo-LDH

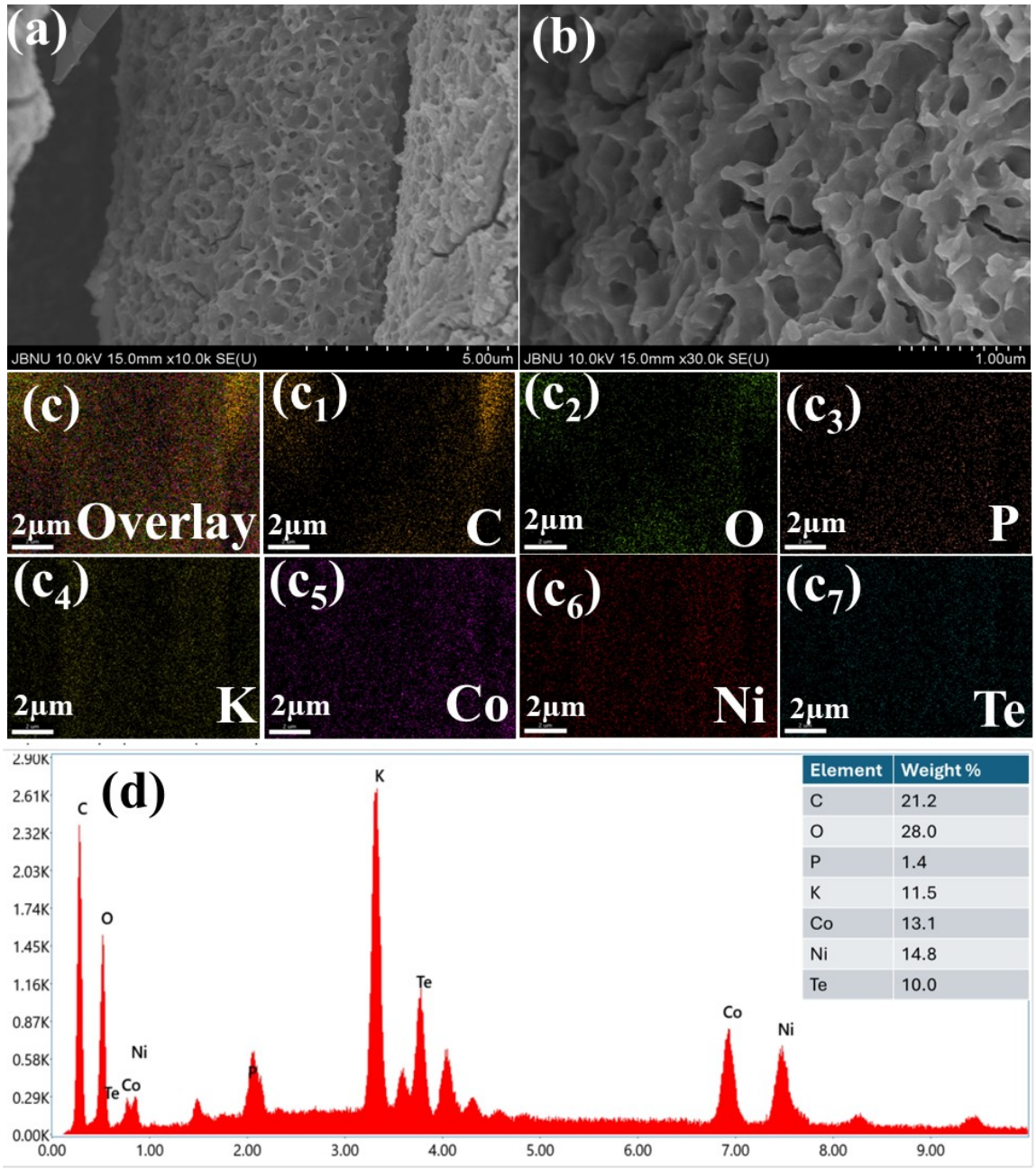

Element	Weight %
C	21.2
O	28.0
P	1.4
K	11.5
Co	13.1
Ni	14.8
Te	10.0

Figure S6. FESEM image, EDX, and corresponding elemental mapping of P-doped $NiTe_2/CoTe_2$@CC after OER stability test.

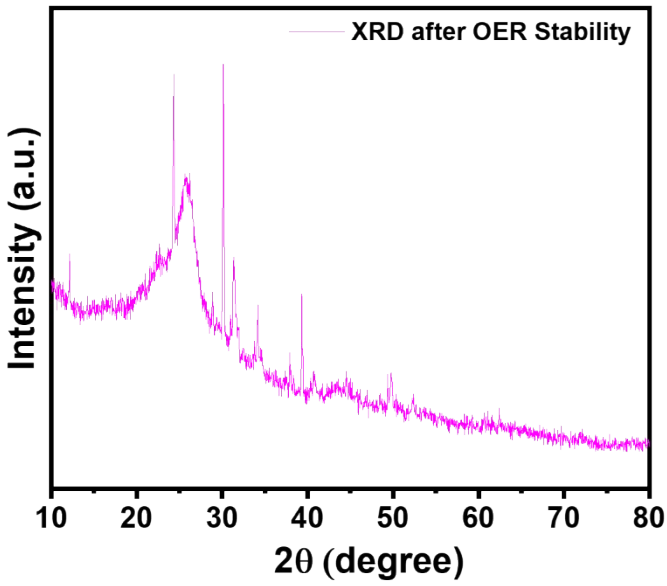

Figure S7. XRD pattern of P-doped $Nite_2/CoTe_2$@CC after OER stability test.

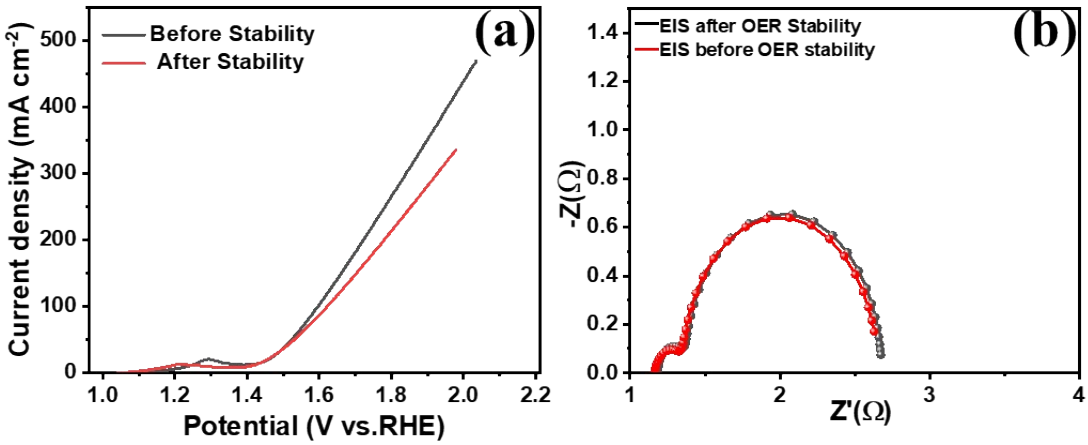

Figure S8. Comparison of (a) LVS and (b) EIS spectra before and after OER stability test.

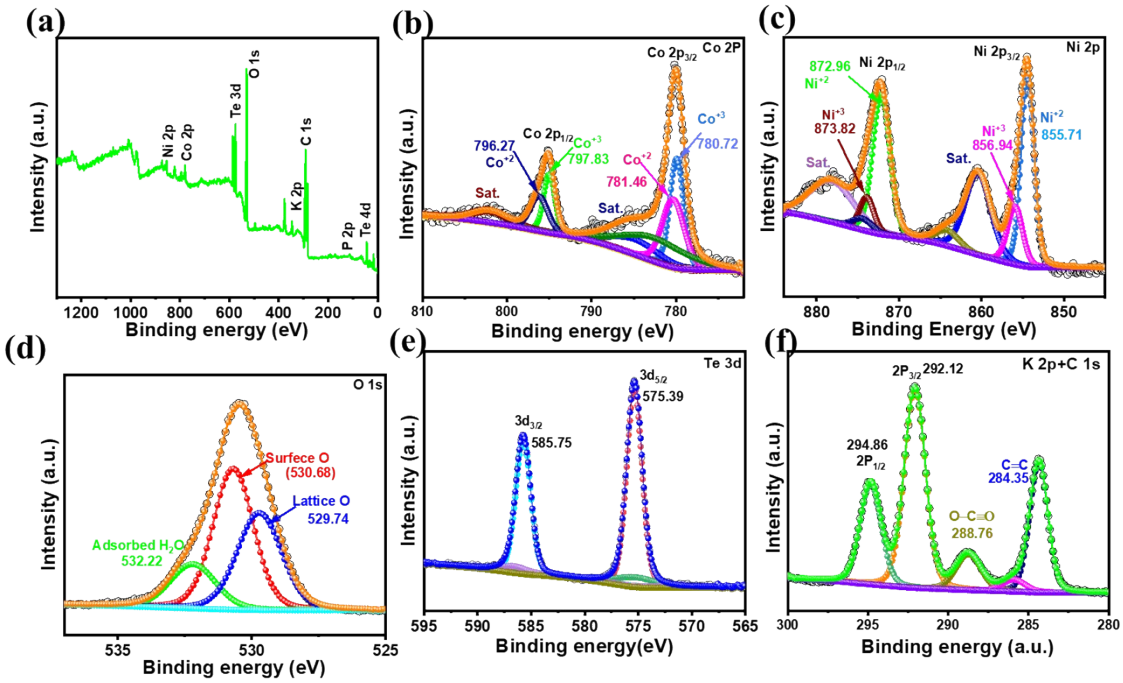

Figure S9. XPS survey Spectra (a), high resolution XPS spectra of (b) Co 2p, (c) Ni 2p, (d) O 1s, (e) Te 3d, (f) K2P+C 1s after OER stability test.

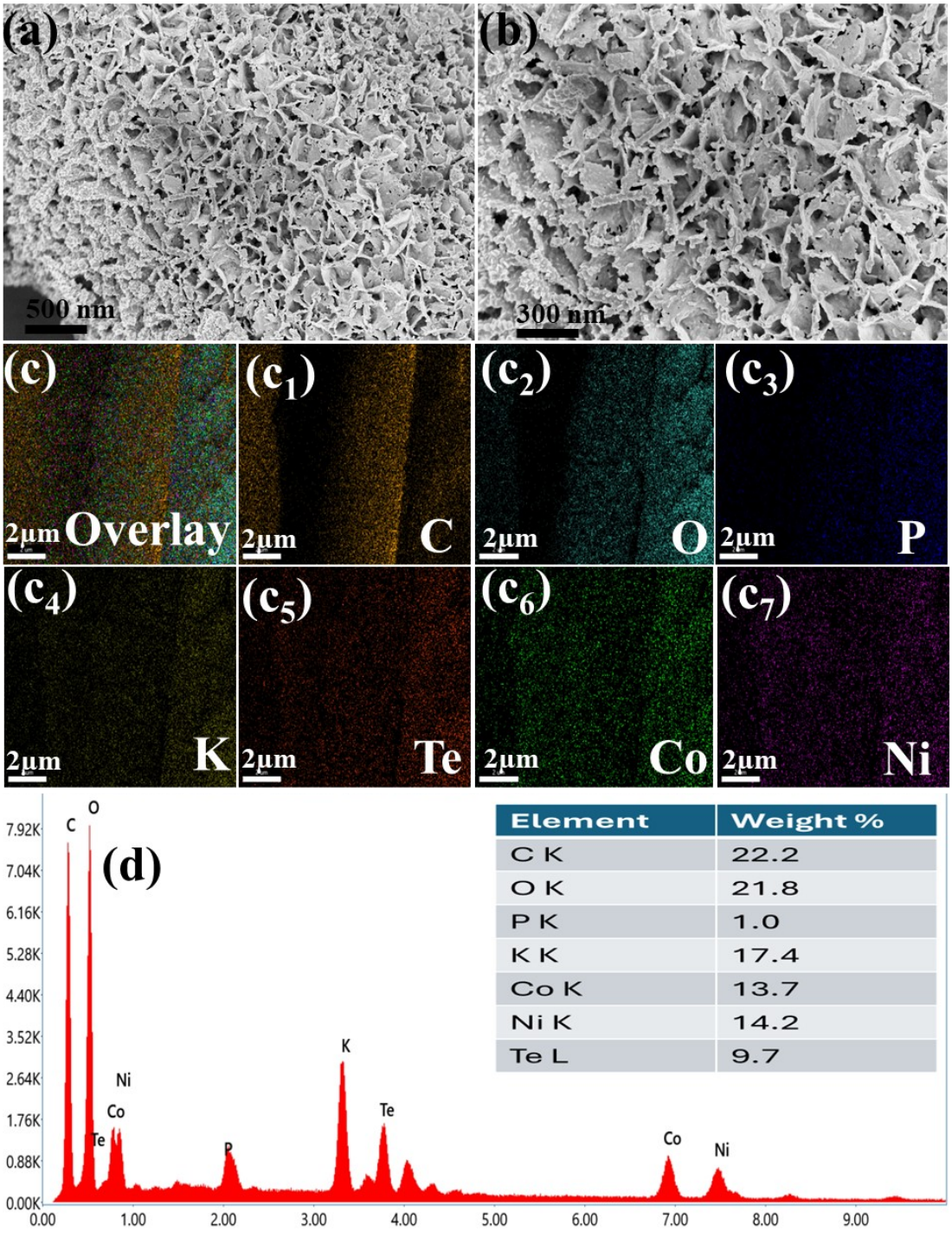

Figure S10. FESEM image, EDX, and corresponding elemental mapping of P-doped $NiTe_2/CoTe_2$@CC after HER stability test.

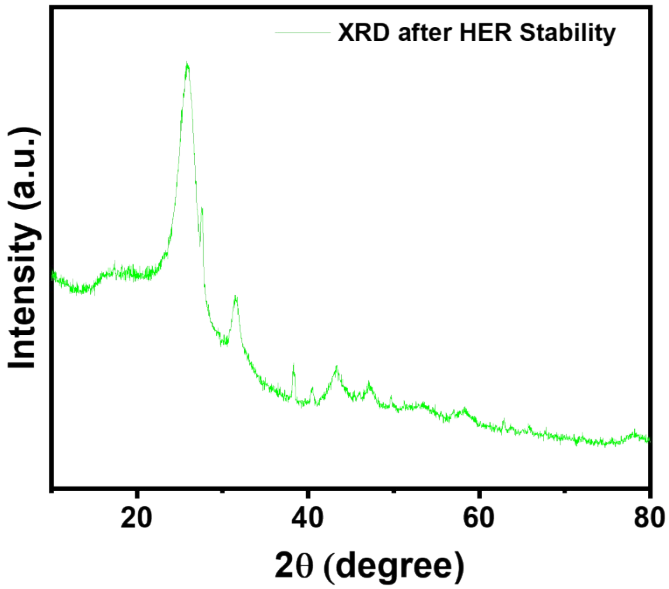

Figure S11. XRD patterns of P-doped $NiTe_2/CoTe_2$@CC after HER stability test

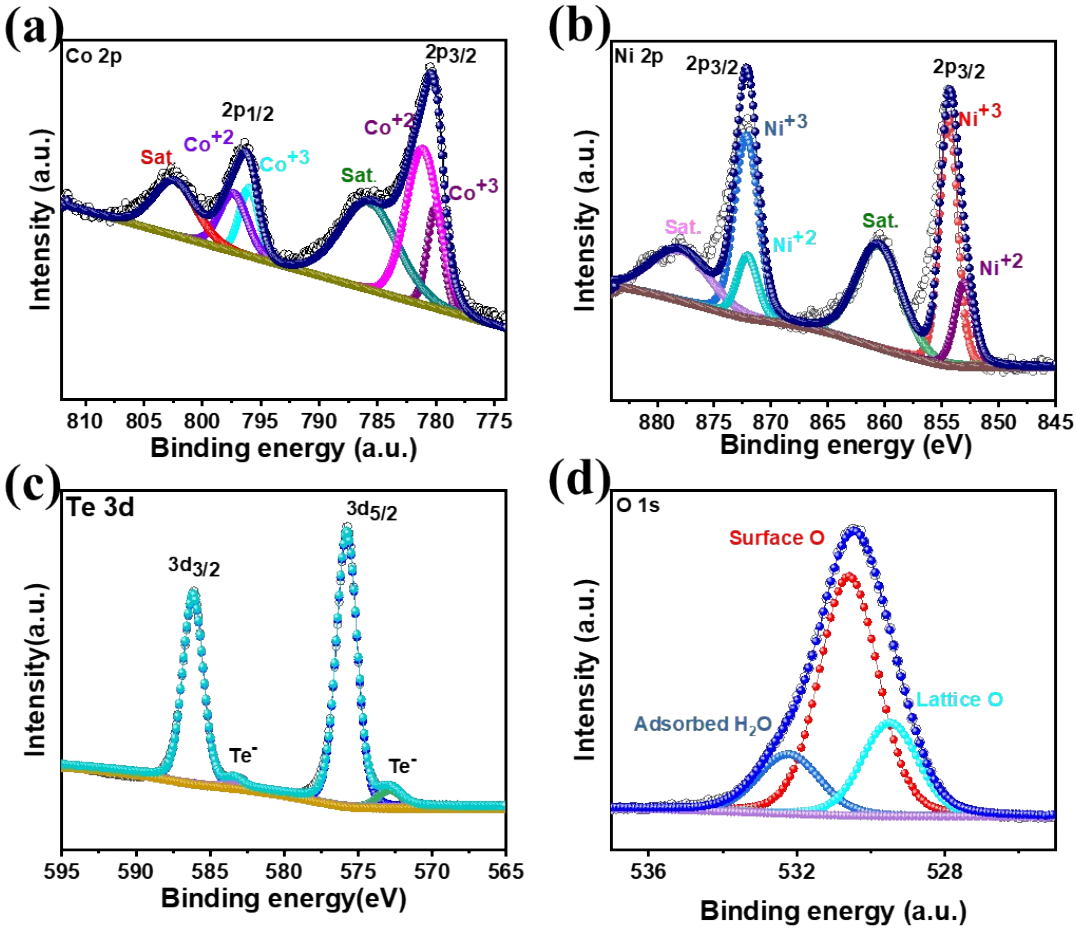

Figure S12. High resolution XPS spectra of (a) Co 2p, (b) Ni2p, (c) Te 3d, (d) O 1s after HER stability test

Table S1. Comparison of OER performance with recently reported electrocatalysts.

S.N.	Electrocatalysts	Substrate	electrolyte	Overpotential(mV)	Tafel slope ($mV\ dec^{-1}$)	Ref.
1	H-$CoTe_2$/$NiTe_2$	GC	1.0M KOH	320@10mA cm^{-2}	64.8	[1]
2	N- Fe_2O_3/$NiTe_2$	Ni foam	1.0M KOH	253@10mA cm^{-2}	57.7	[2]
3	CoTe/Co_3O_4	GC	1.0M KOH	287 @10mA cm^{-2}	69	[3]
4	CoTe/MnO_2/BN	CP	1.0M KOH	273@10mA cm^{-2}	81	[4]
5	Co@0.2gNiCoTe_2-240	Co foam	1.0M KOH	280@10mA cm^{-2}	34	[5]
6	S_{15}–CoTe	NF	1.0M KOH	255@10mA cm^{-2}	54.7	[6]
7	$CoTe_2$@N-GC	CP	1.0M KOH	300@10mA cm^{-2}	90	[7]
9	Fe-$NiTe_2$/Ni_2P	NF	1.0M KOH	190@10mA cm^{-2}	102	[8]
10	Fe-NiTe/$NiTe_2$	GC	1.0M KOH	284@10mA cm^{-2}	49	[9]
11	**P-doped $NiTe_2$/$CoTe_2$**	**CC**	**1.0M KOH**	**251@ 50mA cm^{-2}**	**46**	**This work**

Table S2. Comparison of HER performance with recently reported electrocatalysts

S.N.	Electrocatalysts	Substrate	electrolyte	Overpotential(mV) @10 mA cm^{-2}	Tafel slope ($mV\ dec^{-1}$)	Ref.
1	$NiCoSe_x$	NF	1.0M KOH	83	127	[10]
2	NiTe-$Ni(OH)_2$	NF	1.0 M KOH	129	31.5	[11]
3	N- $Fe_2O_3/NiTe_2$	NF	1.0 M KOH	70	47	[2]
4	$CoTe/CoNiSe_2$	NF	1.0 M KOH	140	78	[12]
5	CoP-$CoTe_2$ NWs	CP	1.0 M NaOH	178		[13]
6	$CoTe_2$–WTe_2	NF	1.0 M KOH	178	96	[14]
7	NiCo-MOFs	NF	1.0 M KOH	125	78	[15]
8	Fe-$CoSe_2$	GC	0.5 M KOH	157	112	[16]
9	$CoTe_2$/CoP	Ti mesh	1.0 M KOH	80	57	[17]
10	**P-doped $NiTe_2/CoTe_2$**	**CC**	**1.0 M KOH**	**83.53**	**68**	**This work**

Table 3. Comparison of overall water-splitting performance with recently reported electrocatalysts.

S.N.	Electrocatalysts	Substrate	Electrolyte	Cell Voltage (V) @10 mA cm^{-2}	Ref.
1	N- $Fe_2O_3/NiTe_2$	Ni Foam	1.0 M KOH	1.54	3
2	CoP Nanoframes	Ni foam	1.0 M KOH	1.65	18
3	$CoNi/CoFe_2O_4$	Ni foam	1.0 M KOH	1.57	19
4	$NiSe-NiSe_2$	Ni foam	1.0 M KOH	1.6	20
5	P-doped $NiSe_2$	Ni foam	1.0 M KOH	1.62	21
6	Cr-$NiSe_2$-N	Ni foam	1.0 M KOH	1.59	22
7	CoTe	Ni foam	1.0 M KOH	1.71	23
8	$CoTe_2$-WTe_2	Ni foam	1.0 M KOH	1.52	14
9	1T-Co-$WS_2/NiTe_2$	Ni foam	1.0 M KOH	1.52	24
10	**P-doped $NiTe_2/CoTe_2$**	**Carbon Cloth**	**1.0 M KOH**	**1.59**	**This work**

Water splitting video_H cell.mp4

Video S1: Real time observation of gas bubble evolution during HER and OER in an H-Cell using P-doped $NiTe_2/CoTe_2$ (+, -) as both anode and cathode.

References:

1. Liu, M.; Li, Q.; Xiao, X.; Ma, X.; Xu, X.; Yin, Y.; Zhang, B.; Ding, M.; Zou, J.; Jiang, B., CoTe2/NiTe2 heterojunction embedded in N-doped hollow carbon nanoboxes as high-efficient ORR/OER catalyst for rechargeable zinc-air battery. *Chemical Engineering Journal* **2024,** *486*, 150256.
2. Li, W.; Deng, Y.; Luo, L.; Du, Y.; Cheng, X.; Wu, Q., Nitrogen-doped Fe2O3/NiTe2 as an excellent bifunctional electrocatalyst for overall water splitting. *Journal of Colloid and Interface Science* **2023,** *639*, 416-423.
3. Rani, P.; Ahmed, I.; Dastider, S. G.; Biswas, R.; Mondal, K.; Haldar, K. K.; Patole, S. P.; Alegaonkar, P. S., Exploring the Role of CoTe/Co3O4 Composite Catalyst for Enhanced Oxygen Evolution Reaction. *ACS Applied Engineering Materials* **2023,** *1* (12), 3389-3402.
4. Rani, P.; Biswas, R.; Dutta, A.; Alegaonkar, P. S., Hierarchical CoTe/MnO2/BN Ternary Composite Exhibiting Energy-Efficient O2 Evolution in Water. *Energy & Fuels* **2024,** *38* (17), 16809-16819.
5. Qi, Y.; Yang, Z.; Peng, S.; Wang, M.; Bai, J.; Li, H.; Xiong, D., Self-supported cobalt–nickel bimetallic telluride as an advanced catalyst for the oxygen evolution reaction. *Inorganic Chemistry Frontiers* **2021,** *8* (18), 4247-4256.
6. Pi, Z.; Hao, J.; Kuang, S.; Shi, R.; Li, X.; Wang, J.; Lin, H.; Nie, M.; Li, Q., In-situ route to sulfur-doped cobalt telluride nanowires for efficient oxygen evolution in alkaline. *International Journal of Hydrogen Energy* **2024,** *93*, 84-91.
7. Liu, M.; Lu, X.; Guo, C.; Wang, Z.; Li, Y.; Lin, Y.; Zhou, Y.; Wang, S.; Zhang, J., Architecting a Mesoporous N-Doped Graphitic Carbon Framework Encapsulating CoTe2 as an Efficient Oxygen Evolution Electrocatalyst. *ACS Applied Materials & Interfaces* **2017,** *9* (41), 36146-36153.
8. Li, W.; Yu, X.; Luo, L.; Du, Y.; Wu, Q., Fe-doped NiTe2/Ni2P grown in situ on Ni foam as an efficient electrocatalyst for oxygen evolution reaction. *Journal of Alloys and Compounds* **2022,** *917*, 165369.
9. Zhang, Y.; Wang, B.; Bi, K.; Tian, F.; Wang, C., Self-assembly of 2D Fe-doped NiTe/NiTe2 heterostructure for boosted oxygen evolution. *Molecular Catalysis* **2023,** *550*, 113586.
10. Lin, X.; Zhong, H.; Hu, W.; Du, J., Nickel–Cobalt Selenide Electrocatalytic Electrode toward Glucose Oxidation Coupling with Alkaline Hydrogen Production.

Inorganic Chemistry **2023,** *62* (26), 10513-10521.
11. Li, Q.; Huang, N.; Zhu, W.; Ma, H.; Du, J.; He, X.; Wang, S.; Li, C.; Wang, W.; Weng, Y., Preparation of NiTe-Ni(OH)2/NF active cathode material as an electrocatalyst for hydrogen evolution. *Journal of Alloys and Compounds* **2024,** *990*, 174458.
12. Atallah, D.; Ali Shah, T.; Rodríguez-Ortiz, G.; Nauman Ullah, M.; Mahmood, F.; Shazly, G. A.; Waqas, M., CoTe Tailored CoNiSe2 Nanostructures as CoTe/CoNiSe2 Hybrids Facilitating Bifunctional Behavior in Overall Water Splitting. *ACS Applied Energy Materials* **2024,** *7* (22), 10693-10700.
13. Amorim, I.; Xu, J.; Zhang, N.; Yu, Z.; Araújo, A.; Bento, F.; Liu, L., Dual-phase CoP−CoTe2 nanowires as an efficient bifunctional electrocatalyst for bipolar membrane-assisted acid-alkaline water splitting. *Chemical Engineering Journal* **2021,** *420*, 130454.
14. Velpandian, M.; Ragunathan, A.; Ummethala, G.; Krishna Malladi, S. R.; Meduri, P., Low-Potential Overall Water Splitting Induced by Engineered CoTe2–WTe2 Heterointerfaces. *ACS Applied Energy Materials* **2023,** *6* (11), 5968-5978.
15. Sreekanth, T. V. M.; Kiran, G. K.; Kim, J.; Yoo, K., NiCo bimetallic metal-organic framework (NiCo-MOFs) with distinct morphologies for efficient HER activity. *Inorganic Chemistry Communications* **2024,** *161*, 112128.
16. Samal, R.; Mane, P.; Chakraborty, B.; Late, D.; Rout, C. S., Trends of earth-abundant transition metal-doped in CoSe microstructures towards improved water splitting and supercapacitor applications. *International Journal of Energy Research* **2022,** *46* (15), 24588-24601.
17. Yang, L.; Cao, X.; Wang, X.; Wang, Q.; Jiao, L., Regulative electronic redistribution of CoTe2/CoP heterointerfaces for accelerating water splitting. *Applied Catalysis B: Environmental* **2023,** *329*, 122551.
18. Ji, L.; Wang, J.; Teng, X.; Meyer, T. J.; Chen, Z., CoP Nanoframes as Bifunctional Electrocatalysts for Efficient Overall Water Splitting. *ACS Catalysis* **2020,** *10* (1), 412-419.
19. Li, S.; Sirisomboonchai, S.; Yoshida, A.; An, X.; Hao, X.; Abudula, A.; Guan, G., Bifunctional CoNi/CoFe2O4 /Ni foam electrodes for efficient overall water splitting at a high current density. *Journal of Materials Chemistry A* **2018,** *6* (39), 19221-19230.
20. Fan, J.; Shen, L.; Zhao, C.; Wang, Z.; Tu, Z.; Hu, J.; Yan, C., Dual-phase NiSe–NiSe2 constructs rapid hydrogen evolution channels by phase control achieve high-performance water electrolysis catalyst. *International Journal of Hydrogen Energy* **2025,**

119, 397-405.
21. Lin, J.; Wang, H.; Cao, J.; He, F.; Feng, J.; Qi, J., Engineering Se vacancies to promote the intrinsic activities of P doped NiSe2 nanosheets for overall water splitting. *Journal of Colloid and Interface Science* **2020,** *571*, 260-266.
22. Zheng, X.; Sun, S.; Liu, Y.; Li, D.; Tian, D.; Zhu, J.; Jiang, D., Synergistic modulation of NiSe2 by doping with chromium and nitrogen for high-efficiency overall water splitting. *Applied Surface Science* **2023,** *609*, 155406.
23. Nath, M.; De Silva, U.; Singh, H.; Perkins, M.; Liyanage, W. P. R.; Umapathi, S.; Chakravarty, S.; Masud, J., Cobalt Telluride: A Highly Efficient Trifunctional Electrocatalyst for Water Splitting and Oxygen Reduction. *ACS Applied Energy Materials* **2021,** *4* (8), 8158-8174.
24. Paudel, D. R.; Pan, U. N.; Ghising, R. B.; Dhakal, P. P.; Dinh, V. A.; Wang, H.; Kim, N. H.; Lee, J. H., Interface modulation induced by the 1T Co-WS2 shell nanosheet layer at the metallic NiTe2/Ni core–nanoskeleton: Glib electrode-kinetics for HER, OER, and ORR. *Nano Energy* **2022,** *102*, 107712.